Tracking on the Product Manifold of Shape and Orientation for Tractography from Diffusion MRI *

Yuanxiang Wang
Department of ECE
University of Florida, Gainesville, FL
yuawang@cise.ufl.edu

Hesamoddin Salehian, Guang Cheng and Baba C. Vemuri
Department of CISE
University of Florida, Gainesville, FL
{salehian,gcheng,vemuri}@cise.ufl.edu

Abstract

Tractography refers to the process of tracing out the nerve fiber bundles from diffusion Magnetic Resonance Images (dMRI) data acquired either in vivo or ex-vivo. Tractography is a mature research topic within the field of diffusion MRI analysis, nevertheless, several new methods are being proposed on a regular basis thereby justifying the need, as the problem is not fully solved. Tractography is usually applied to the model (used to represent the diffusion MR signal or a derived quantity) reconstructed from the acquired data. Separating shape and orientation of these models was previously shown to approximately preserve diffusion anisotropy (a useful bio-marker) in the ubiquitous problem of interpolation. However, no further intrinsic geometric properties of this framework were exploited to date in literature. In this paper, we propose a new intrinsic recursive filter on the product manifold of shape and orientation. The recursive filter, dubbed IUKFPro, is a generalization of the unscented Kalman filter (UKF) to this product manifold. The salient contributions of this work are: (1) A new intrinsic UKF for the product manifold of shape and orientation. (2) Derivation of the Riemannian geometry of the product manifold. (3) IUKFPro is tested on synthetic and real data sets from various tractography challenge competitions. From the experimental results, it is evident that IUKFPro performs better than several competing schemes in literature with regards to some of the error measures used in the competitions and is competitive with respect to others.

1. Introduction

Diffusion Weighted Magnetic Resonance Imaging (DWMRI) is a relatively nascent Magnetic Resonance imaging technique that allows one to non-invasively probe the neuronal pathways in the central nervous system. Numerous algorithms published in the literature attempt to reveal the fibrous structures in the brain, spinal cord and other parts of the anatomy. The process of inferring and tracing out the neuronal fiber bundles is called tractography. The tractography methods in literature primarily fall in two main categories, deterministic and probabilistic. However, the probabilistic methods are far more computationally expensive than the aforementioned deterministic techniques, thus in this paper we limit ourselves to the deterministic methods, and refer the reader to [3] and the references therein for the probabilistic methods.

The streamline algorithm is one of the most popular deterministic tractography technique, where at each voxel the direction of the underlying neuronal fiber is estimated and tracked [15]. For instance, in the Diffusion Tensor Imaging (DTI) where the DWMR signal $S(\mathbf{g})$ decay along the magnetic field gradient direction $\mathbf{g}$ is modeled by a single zero mean Gaussian, i.e., $S(\mathbf{g}) = S_0 \exp(-\mathbf{g}^t \mathbf{D} \mathbf{g})$, where S_0 is the DWMR signal with zero diffusion weighting and $\mathbf{D}$ is the diffusion tensor which is the inverse covariance matrix of the Gaussian, the fibers would be oriented along the largest eigenvector of the diffusion tensor $\mathbf{D}$ [2]. It is however well-known in DWMRI analysis research community that the single Gaussian (mono-exponential) signal decay model characterizing the DTI is incapable of accurately capturing the neuronal pathways in presence of complex fibrous structures, e.g., crossing and kissing fibers, which are often encountered in many locations in the brain and the spinal cord.

To address this shortcoming, some extensions of streamline are proposed based on the reconstruction models from High Angular Resolution Diffusion Imaging (HARDI). Higher order tensors [1], Orientation Distribution Functions (ODFs) [8, 6] are instances of HARDI reconstruction models based on which the streamline is generalized, where in each case, the maxima of the ODF are estimated and the streamline technique is applied to trace out the fiber tracts. Front-propagation approaches are another example of de-

terministic tractography, where white matter fiber bundles are considered as a Riemannian manifold, equipped with a metric derived from the diffusion tensor data [9, 18]. The neuronal fiber tracts are then treated as geodesics using this metric. While robust, these DTI-based models suffer from the same shortcomings mentioned earlier.

Most of the aforementioned fiber tracking methods are based on a two stage procedure, first estimating the underlying model from DWMRI throughout the image, and then tracking based on the estimated model. Recently, authors in [14] proposed a clever multi-tensor (mixture of two zero mean Gaussians – called the bi-tensor model) tractography method using an unscented Kalman filter (UKF), where the multi-tensor estimation and the propagation of directional information were performed simultaneously. This approach provides two important advantages: (1) The reconstruction is only performed along the fiber tracts, which yields a significant computational efficiency since one need not reconstruct the multi-tensors all over the image but only at voxels likely to be on the fiber paths, (2) propagating the most consistent direction to track along achieves smoothness of the tracts being traced using a streamline technique. The streamline method implicitly regularizes the tracts by using the most consistent direction from the smooth estimates of tensors obtained from the UKF. However, this UKF-based tractography method was not intrinsic to the space of diffusion tensors, a drawback that may lead to non-positive definiteness of the estimated diffusion tensors. It is well-known that the diffusion tensors belong to the space of $(n \times n)$ symmetric positive-definite (SPD) matrices, denoted by $P(n)$ that is not a Euclidean space, but a negatively curved Riemannian manifold [16]. In this context, in [10, 23] generalizations of UKF to Riemannian manifolds were proposed. While these methods are quite general extensions, there are some technical problems that are not fully considered in these works and will be discussed in details in Section 2. While none of the above intrinsic UKFs are used in tractography applications, authors in [5] presented an extension of UKF to $P(n)$ and applied it to tractography. The work presented in this paper is however quite distinct as will be evident subsequently.

Recently, in [4, 17], it was shown that the Fisher-Rao (Riemannian) metric when used for interpolation of ODFs fails to preserve clinically useful properties such as the fractional anisotropy (FA) – a scalar-valued function of the eigenvalues of the diffusion tensor **D**[2]. Fig. 1 illustrates this phenomena for the task of interpolation of diffusion tensors, where interpolation using different metrics is performed between two tensors having the same FA value. It can be seen that the Euclidean, LogEuclidean and GL-invariant Riemannian metrics, used in [5], all produce interpolated tensors whose shapes are different from those of the end point tensors. Lack of preservation of anisotropy mea-
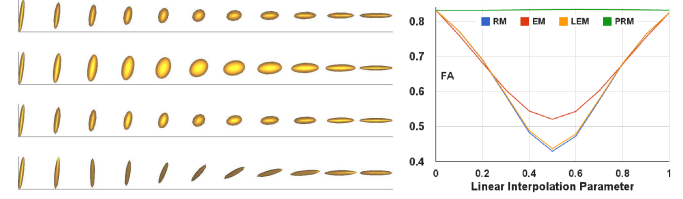

Figure 1: Left shows the tensor interpolation, using the Riemannian GL-invariant metric (1st row), Euclidean metric (2nd row), LogEuclidean metric (3rd row) and the product Riemannian metric of shape & orientation (4th row), abbreviated as RM, EM, LEM & PRM, respectively. Right shows comparison of their FA-values.

sures will obviously lead to inaccuracies in tractography.

To address this issue, a clever solution was proposed for the case of ODFs in [4, 17] involving the concept of treating the orientation of ODFs separately from their shape for interpolation and denoising problems. To find the interpolated path between two given ODFs (possibly located at distinct points in an ODF field), they minimize the Fisher-Rao distance between all possible rotations of two ODFs along with a regularization term which seeks to keep the rotation small so that the shape is preserved in the interpolant. Authors in both the articles do not however explore the full geometry of the product space of shape and orientations further.

Our work is also based on the idea of separating the shape and orientation and then additionally considers the Riemannian product space of shape and orientation, but for the bi-tensor model and not the ODFs. However, similar analysis is also applicable to the ODFs and the ensemble average propagator (EAP) which is defined as the Fourier transform of the DWMR signal. Accordingly, we would like to emphasize that our method is significantly different from the one reported in [5], because in their work the idea of separating shape and orientation was not taken into account, leading to less accurate tractography results compared to ours. These results are presented in Section 3.

Therefore, *our key contributions are:* we derive the Riemannian geometry of this product space by imposing a bi-invariant Riemannian metric, including the log and exp maps and the geodesic equations. In addition, we develop a novel recursive unscented Kalman filter on this product space and apply it to the publicly available DWMR realistic phantom data [7], our own synthetic data and real DWMR data from human brains. The accuracy of our tractography results on the fibercup challenge data [7] are better than those published in literature for the spatial distance measures used to evaluate the tractography in [7] and competitive in the other measures used for evaluation. As an illustration, we present results of interpolation using the product space metric used in our approach in Fig. 1. It is visually evident from the figure that the our approach preserves the shape of the tensors along the interpolated path better than our competition.

The rest of the paper is organized as follows: in sec-

tion 2, we first provide the motivation for using UKF in the tractography problem. Then, the mathematical derivation of the Riemannian geometry of the shape & orientation product manifold are presented followed by the intrinsic unscented Kalman filter on this product manifold. Section 3 includes the synthetic and real data experiments showing the effectiveness and accuracy of the new method. Section 4 contains the conclusions.

2. IUKFPro: Intrinsic UKF on the Product Space of Shape & Orientation

As described earlier, in tractography the neuronal pathways from imaged tissue are traced out based on the given DWMR signal. Therefore, care must be taken to reconstruct the underlying fiber direction accurately at each voxel in the DWMR data. In most of the existing techniques, e.g., [8, 9], first a model is fitted to the MR signal, the fiber pathway direction is computed following which tractography is performed using the estimated direction. It is however more apt to estimate the fiber directions recursively along the fiber. This brings forth two important advantages, (1) the smoothness along the fiber is employed to provide a more accurate estimation of the fiber direction at each voxel, (2) the reconstruction of the tensor (ODF/EAP) is only performed at locations in the image that lie on the fiber, and hence the computational complexity is reduced considerably.

Simultaneous estimation of the tensors at each voxel and propagation of the direction information for tractography can be achieved recursively. Recursive estimation can be easily cast into a state-space formulation as is normally done in control theory literature. From a state-space modeling viewpoint, the tensors and the MR signal at each voxel can be viewed as the system state and observation, respectively. Therefore, a recursive stochastic dynamic filter such as the well known Kalman Filter (KF) is an appealing choice for this problem. KF is a linear filter, and the Extended KF (EKF) is a nonlinear extension, wherein the probability distribution of the system state is estimated by a Gaussian random variable and propagated through the system dynamics analytically by using a first order linearization of the nonlinear function. EKF however may lead to significant errors in the mean and covariance approximation of the transformed random variable, and in effect lead to divergence of the filter [12]. Compared with KF and the EKF, the Unscented KF (UKF) is a more stable and accurate alternative which uses a set of carefully chosen sample points to accurately approximate the mean and covariance of the Gaussian random variable through the system dynamics. In the tractography problem, we model the diffusion MR signal by a mixture model in the presence of intra-voxel heterogeneity, and we want to estimate the model parameters and propagate the most consistent directional information, simultaneously. Therefore, the UKF is a more appealing

choice for this problem than the KF and EKF.

In this section, we present a novel intrinsic UKF henceforth called IUKFPro, for the case when the system state parameters belong to the product space of shape & orientation. We first introduce the shape & orientation representation of diffusion tensors as a Riemannian product manifold along with its Riemannian geometry. Then, we present a detailed description of IUKFPro in subsequent sections.

2.1. Product Space of Shape & Orientation for representing Diffusion Tensors

Diffusion tensors are $(3, 3)$ symmetric positive definite (SPD) matrices. The eigen-decomposition of an SPD matrix can be expressed as, $\mathbf{D} = \mathbf{U}\Lambda\mathbf{U}^T$ wherein, the component $\mathbf{U} \in \mathrm{SO}(n)$, and $\mathrm{SO}(n)$ is the *special orthogonal group* and the component Λ, a *real diagonal matrix with positive entries*. Here $\mathbf{U}$ contains the orientation information of a diffusion tensor in terms of its eigen vectors, and Λ conveys the shape information of a diffusion tensor expressed in terms of its eigenvalues. Let us denote the space of Λ by $\mathbf{H}_n$, and it is known that $\mathbf{H}_n$ is an connected Lie group isomorphic to $\mathbf{R}_n^+$. We propose a natural shape & orientation representation of a diffusion tensor by the construction of a Riemannian product manifold $\mathbf{M} = \mathrm{SO}(n) \times \mathbf{H}_n$.

As pointed out in [13], $\mathrm{SO}(n)$ admits a canonical bi-invariant Riemannian metric, and $\mathbf{H}_n$ is equipped with a bi-invariant Riemannian metric namely the *Hyperbolic Metric*. The two bi-invariant Riemannian metrics are given by:

$$g_S = \mathrm{tr}[\dot{\mathbf{P}}^T \dot{\mathbf{P}}]; \; g_{\mathbf{H}} = \mathrm{tr}[(\mathbf{Q}^{-1}\dot{\mathbf{Q}})^T(\mathbf{Q}^{-1}\dot{\mathbf{Q}})], \quad (1)$$

where $\mathbf{P} \in \mathrm{SO}(n), \dot{\mathbf{P}} \in \mathrm{T}_{\mathbf{P}}\mathrm{SO}(n)$, $\mathbf{Q} \in \mathbf{H}_n, \dot{\mathbf{Q}} \in \mathrm{T}_{\mathbf{Q}}\mathbf{H}_n$, and $\mathrm{T}_{\mathbf{P}}\mathrm{SO}(n), \mathrm{T}_{\mathbf{Q}}\mathbf{H}_n$ are the tangent spaces of $\mathbf{P} \in \mathrm{SO}(n)$ and $\mathbf{Q} \in \mathbf{H}_n$, respectively. Given the two Riemannian metrics in equation (1), it is easy to show from basic differential geometry [13] that the *product Riemannian metric* on $\mathbf{M}$ is given by $g_{\mathbf{M}} = g_S \oplus g_{\mathbf{H}}$. Since g_S and $g_{\mathbf{H}}$ are both bi-invariant, the product Riemannian metric $g_{\mathbf{M}}$ is also bi-invariant. In addition, following [13], the geodesic between two points $(\mathbf{p}_1, \mathbf{q}_1)$ and $(\mathbf{p}_2, \mathbf{q}_2)$ on $\mathbf{M}$ is given by $\gamma_{(\mathbf{p}_1, \mathbf{q}_1),(\mathbf{p}_2, \mathbf{q}_2)}(t) = \left(\mathbf{p}_1(\mathbf{p}_1^T\mathbf{p}_2)^t, \mathbf{q}_1(\mathbf{q}_1^{-1}\mathbf{q}_2)^t\right)$. where $\mathbf{p}_1, \mathbf{p}_2 \in \mathrm{SO}(n), \mathbf{q}_1, \mathbf{q}_2 \in \mathbf{H}_n, t \in [0, 1]$. With this geodesic in the product manifold $\mathbf{M}$, we can derive the *Exponential Map* and *Log Map* on $\mathbf{M}$, which are given by:

$$\mathrm{Exp}_{(\mathbf{p},\mathbf{q})}(\mathbf{v}_1, \mathbf{v}_2) = \left(\mathbf{p}\exp(\mathbf{p}^T\mathbf{v}_1), \mathbf{q}\exp(\mathbf{q}^{-1}\mathbf{v}_2)\right)$$
$$\mathrm{Log}_{(\mathbf{p}_1,\mathbf{q}_1)}(\mathbf{p}_2, \mathbf{q}_2) = \left(\mathbf{p}_1\log(\mathbf{p}_1^T\mathbf{p}_2), \mathbf{q}_1\log(\mathbf{q}_1^{-1}\mathbf{q}_2)\right) \quad (2)$$

where $\mathbf{p} \in \mathrm{SO}(n), \mathbf{q} \in \mathbf{H}_n, \mathbf{v}_1 \in \mathrm{T}_{\mathbf{p}}\mathrm{SO}(n), \mathbf{v}_2 \in \mathrm{T}_{\mathbf{p}}\mathbf{H}(n)$ in the *Exponential* map, $\mathbf{p}_1, \mathbf{p}_2 \in \mathrm{SO}(n), \mathbf{q}_1, \mathbf{q}_2 \in \mathbf{H}_n$ in the *Log* map, and $\exp(\cdot)$ & $\log(\cdot)$ are the matrix exponential & logarithm operations, respectively.

2.2. The State Transition and Observation Models in IUKFPro

We are now ready to present the IUKF for the product manifold $\mathbf{M}$. This filter will allow us to simultaneously estimate and track the fibers by using a bi-tensor model [22] for the diffusion signal. To completely specify the IUKF, we need to define the state transition and observation models as well as the update equations and the Kalman gain. The state transition model on $\mathbf{M}$ is based on the natural *direct product of Lie group operations* in $\mathrm{SO}(n)$ and $\mathbf{H}_n$ and the *LogNormal distribution* for the noise, in the case of diffusion tensor, when $n = 3$. We employ a bi-tensor (sum of two Gaussians) model [22] as the observation model [14] to capture crossing fiber geometries at a voxel. The state transition model at iteration k is given by the following equation:

$$\left(\mathbf{U}_1^{(k+1)}, \Lambda_1^{(k+1)}\right) = \mathrm{Exp}_{\left(\mathbf{F}_1\mathbf{U}_1^{(k)}, \mathbf{F}_2\Lambda_1^{(k)}\right)}\left(\mathbf{a}_1^{(k)}, \mathbf{b}_1^{(k)}\right),$$

$$\left(\mathbf{U}_2^{(k+1)}, \Lambda_2^{(k+1)}\right) = \mathrm{Exp}_{\left(\mathbf{F}_1\mathbf{U}_2^{(k)}, \mathbf{F}_2\Lambda_2^{(k)}\right)}\left(\mathbf{a}_2^{(k)}, \mathbf{b}_2^{(k)}\right), \quad (3)$$

where $\mathbf{F}_1, \mathbf{F}_2$ are state transition operations in $\mathrm{SO}(3)$ and $\mathbf{H}_3$, respectively. $\left(\mathbf{a}_1^{(k)}, \mathbf{b}_1^{(k)}\right)$ and $\left(\mathbf{a}_2^{(k)}, \mathbf{b}_2^{(k)}\right)$ are the Gaussian distributed state transition noise in $\mathrm{T}_{\left(\mathbf{U}_1^{(k)}, \Lambda_1^{(k)}\right)}\mathbf{M}$ and $\mathrm{T}_{\left(\mathbf{U}_2^{(k)}, \Lambda_2^{(k)}\right)}\mathbf{M}$. "$\mathrm{Exp}_{(\cdot)}(\cdot)$" is the Exponential Map in (2). In the state transition model, we assume that the two state transition noise models are independent of each other and of the previous state. This is because in diffusion MRI, the signal at each voxel in the presence of an inhomogeneity caused by crossing fibers is commonly modeled by assuming that the sum total signal at a voxel is caused by mixing of two or more independent sources. We denote by $\mathbf{Q}_1^{(k)}$ and $\mathbf{Q}_2^{(k)}$ the covariance matrices of the two state transition noise models of dimension 6-by-6 for the tangent vectors in $\mathrm{T}_{\left(\mathbf{U}_i^{(k)}, \Lambda_i^{(k)}\right)}\mathbf{M}$. Note that in [10, 23] a constant state transition noise covariance tensor is assumed over a Riemannian manifold to apply an IUKF. However, this is not a valid assumption for an IUKF as evident from the discussion below. Let us denote an initial matrix-variate random variable by $\mathbf{X}_0$ and the product group operation by $\mathbf{F}$ respectively. The explicit forms for these are given by,

$$\mathbf{X}_0 = \mathrm{Exp}_{(\mu_\mathbf{U}, \mu_\Lambda)}(\mathbf{v}_\mathbf{U}, \mathbf{v}_\Lambda), \quad \mathbf{F} = \begin{bmatrix} \mathbf{F}_1 & 0 \\ 0 & \mathbf{F}_2 \end{bmatrix} \quad (4)$$

wherein $\mathbf{v}_\mathbf{U} \in \mathrm{T}_{\mu_\mathbf{U}}\mathrm{SO}(3)$, $\mathbf{v}_\Lambda \in \mathrm{T}_{\mu_\Lambda}\mathbf{H}_3$. Denote $\mu = [\mu_\mathbf{U}^T, \mu_\Lambda^T]^T$, $\mathbf{v} = [\mathbf{v}_\mathbf{U}^T, \mathbf{v}_\Lambda^T]^T$, and $\mathbf{v}$ is from zero-mean Gaussian distribution with covariance matrix $\mathbf{Q}$. Then, after the coordinate transform, the new random variable $\mathbf{X} = \mathbf{F}\mathbf{X}_0 = \mathrm{Exp}_{\mathbf{F}\mu}(\mathbf{F}\mathbf{v})$. The covariance matrix of $\mathbf{F}\mathbf{v}$ will be $\mathbf{Q}(\mathbf{F}) = (\mathbf{I} \otimes \mathbf{F})\mathbf{Q}(\mathbf{I} \otimes \mathbf{F})^T$, where $\mathbf{I}$ is the identity matrix, and $\otimes$ denotes the Kronecker product. Therefore, the state transition noise covariance tensor should not be con-

stant over the manifold and should be changed by the induced group operation. In addition, in [10] the use of parallel transport approximated by Schild's ladder method via a sequence of exponential maps followed by a Log map is computationally more expensive than a single Log map operation in our approach. Further, no accuracy measures of their approximation as a function of data variance was reported.

As mentioned before, the observation model is based on the bi-tensor model and given by:

$$Y_n^{(k)} = \frac{Y_0}{2}\left(e^{-b_n\mathbf{g}_n^T\mathbf{U}_1^{(k)}\Lambda_1^{(k)}\mathbf{U}_1^{(k)T}\mathbf{g}_n} + e^{-b_n\mathbf{g}_n^T\mathbf{U}_2^{(k)}\Lambda_2^{(k)}\mathbf{U}_2^{(k)T}\mathbf{g}_n}\right) + r_n^{(k)}$$

$$(5)$$

where $\mathbf{g}_n$ denotes the nth magnetic gradient direction, b_n the corresponding b-value, $Y_n^{(k)}, r_n^{(k)}$ the MR signal and the measurement noise for n^{th} magnetic gradient at the kth iteration, respectively. We assume that the measurements from distinct gradient directions are independent so that the covariance matrix of the observation model for all magnetic gradients, denoted as $\mathbf{R}$, is a diagonal matrix.

2.3. IUKFPro: The Intrinsic Unscented Kalman Filter on M

Since the current dynamic model is based on the shape & orientation product manifold $\mathbf{M}$, we need a non-trivial extension of the IUKF derived in [5]. To begin with, let us first define the augmented state vector for the observation model in equation (5) by

$$\mathbf{X}_k = \left[\mathbf{s}_{\mathbf{U}_1}^{(k)T}, \mathbf{s}_{\mathbf{U}_2}^{(k)T}, \mathbf{s}_{\Lambda_1}^{(k)T}, \mathbf{s}_{\Lambda_2}^{(k)T}, \mathbf{n}_{\mathbf{U}_1}^{(k)T}, \mathbf{n}_{\mathbf{U}_2}^{(k)T}, \mathbf{n}_{\Lambda_1}^{(k)T}, \mathbf{n}_{\Lambda_2}^{(k)T}\right]^T,$$

$$(6)$$

at iteration step k, where $\left(\mathbf{s}_{\mathbf{U}_i}^{(k)}, \mathbf{s}_{\Lambda_i}^{(k)}\right) = \mathrm{Log}_{\widehat{K}(\mathbf{U}_i, \Lambda_i)}(\mathbf{U}_i, \Lambda_i)$ is the representation of the orientation and shape state random vectors in the tangent plane at its Karcher mean $\widehat{K}(\mathbf{U}_i, \Lambda_i)$, and $\left(\mathbf{n}_{\mathbf{U}_i}^{(k)}, \mathbf{n}_{\Lambda_i}^{(k)}\right)$ is the state transition noise vector for $(\mathbf{U}_i, \Lambda_i)$. The covariance matrix for $[\mathbf{s}_{\mathbf{U}_1}^{(k)T}, \mathbf{s}_{\mathbf{U}_2}^{(k)T}, \mathbf{s}_{\Lambda_1}^{(k)T}, \mathbf{s}_{\Lambda_2}^{(k)T}]^T$ is denoted by $\mathbf{P}_{k,\mathbf{U}\Lambda}$. The covariance matrices for $[\mathbf{n}_{\mathbf{U}_1}^{(k)T}, \mathbf{n}_{\Lambda_1}^{(k)T}]^T$ and $[\mathbf{n}_{\mathbf{U}_2}^{(k)T}, \mathbf{n}_{\Lambda_2}^{(k)T}]^T$ are as before, $\mathbf{Q}_1^{(k)}$ and $\mathbf{Q}_2^{(k)}$ respectively. We denote the covariance matrix for the augmented state vector $\mathbf{X}_k$ by $\mathbf{P}_{k,X}$, a block-diagonal matrix composed of $\mathbf{P}_{k,\mathbf{U}\Lambda}$, $\mathbf{Q}_1^{(k)}$, and $\mathbf{Q}_2^{(k)}$ respectively.

The IUKF consists of two stages: prediction stage and an update stage. The prediction & update stages are detailed in Table 1 & 2 respectively.

3. Experiments

To depict the accuracy of our tractography algorithm, we present a set of synthetic data experiments generated at various levels of Riccian noise. Since we know the ground truth for synthesized data we report the reconstruction accuracy

Table 1: The Prediction Stage

(1) Obtain the jth *sigma point* at iteration step k as described in [24]:
$$\mathsf{X}_{k,j} = \left[\mathbf{s}_{\mathbf{U}_{1,j}}^{(k)^T}, \mathbf{s}_{\mathbf{U}_{2,j}}^{(k)^T}, \mathbf{s}_{\Lambda_{1,j}}^{(k)^T}, \mathbf{s}_{\Lambda_{2,j}}^{(k)^T}, \mathbf{n}_{\mathbf{U}_{1,j}}^{(k)^T}, \mathbf{n}_{\mathbf{U}_{2,j}}^{(k)^T}, \mathbf{n}_{\Lambda_{1,j}}^{(k)^T}, \mathbf{n}_{\Lambda_{2,j}}^{(k)^T} \right]^T$$
(7)

(2) Obtain samples $\left(\mathsf{U}_{i,j}^{(k+1)}, \Lambda_{i,j}^{(k+1)} \right)$ on $\mathbf{M}$ from the last iteration's posterior estimates $\left(\hat{\mathsf{U}}_i^{(k)}, \hat{\Lambda}_i^{(k)} \right)$ by two steps: $\left(\tilde{\mathsf{U}}_{i,j}^{(k)}, \tilde{\Lambda}_{i,j}^{(k)} \right) = \mathrm{Exp}_{\left(\hat{\mathsf{U}}_i^{(k)}, \hat{\Lambda}_i^{(k)} \right)} \left(\mathbf{s}_{\mathbf{U}_{i,j}}^{(k)^T}, \mathbf{s}_{\Lambda_{i,j}}^{(k)^T} \right)$, and $\left(\mathsf{U}_{i,j}^{(k+1)}, \Lambda_{i,j}^{(k+1)} \right) = \mathrm{Exp}_{\left(\tilde{\mathsf{U}}_{i,j}^{(k)}, \tilde{\Lambda}_{i,j}^{(k)} \right)} \left(\mathbf{n}_{\mathbf{U}_{i,j}}^{(k)^T}, \mathbf{n}_{\Lambda_{i,j}}^{(k)^T} \right)$.

(3) Compute the predicted mean as a weighted Karcher mean:
$$\left(\hat{\mathsf{U}}_i^{(k+1)}, \hat{\Lambda}_i^{(k+1)} \right) = \mathrm{argmin}_\mu \sum_j w_j \, dist^2 \left(\left(\mathsf{U}_{i,j}^{(k+1)}, \Lambda_{i,j}^{(k+1)} \right), \mu \right)$$
(8)

where $dist(\cdot, \cdot)$ is the geodesic distance, and w_j are the combination weights used from the *sigma point propagation* scheme.

(4) Compute the predicted state covariance: $\mathsf{P}_{\mathbf{U}\Lambda} = \sum_j w_j \mathfrak{U}_j \mathfrak{U}_j^T$. Denote,
$$\mathfrak{U}_j^T = \left[\mathrm{Log}_{\hat{\mathsf{U}}_{1,j}^{(k+1)}} \left(\mathsf{U}_{1,j}^{(k+1)} \right), \mathrm{Log}_{\hat{\mathsf{U}}_{2,j}^{(k+1)}} \left(\mathsf{U}_{2,j}^{(k+1)} \right), \right.$$
$$\left. \mathrm{Log}_{\hat{\Lambda}_{1,j}^{(k+1)}} \left(\Lambda_{1,j}^{(k+1)} \right), \mathrm{Log}_{\hat{\Lambda}_{2,j}^{(k+1)}} \left(\Lambda_{2,j}^{(k+1)} \right) \right], \quad (9)$$

and $\mathsf{Y}_j^{(k+1)}$ as the predicted MR signals for different magnetic gradients via the observation model (5) respectively. The predicted mean of MR signal computed by the standard vector average operation is denoted by $\hat{\mathsf{Y}}^{(k+1)}$.

(5) Compute the predicted observation covariance using: $\mathsf{P}_{\mathbf{ss}}^{(k+1)} = \mathbf{R} + \sum_j w_j \left(\mathsf{Y}_j^{(k+1)} - \hat{\mathsf{Y}}^{(k+1)} \right) \left(\mathsf{Y}_j^{(k+1)} - \hat{\mathsf{Y}}^{(k+1)} \right)^T$, and the cross-correlation matrix between the observation and the states using: $\mathsf{P}_{\mathbf{U}\Lambda\mathbf{s}}^{(k+1)} = \sum_j w_j \mathfrak{U}_j \left(\mathsf{Y}_j^{(k+1)} - \hat{\mathsf{Y}}^{(k+1)} \right)^T$.

Table 2: The Update Stage

1. Compute the *Kalman Gain*: $\mathcal{K}^{(k+1)} = \mathsf{P}_{\mathbf{U}\Lambda\mathbf{s}}^{(k+1)} \mathsf{P}_{\mathbf{ss}}^{(k+1)^{-1}}$
2. Compute the *Innovation*: $\left[\mathbf{z}_{\mathbf{U}_1}^{(k+1)^T}, \mathbf{z}_{\mathbf{U}_2}^{(k+1)^T}, \mathbf{z}_{\Lambda_1}^{(k+1)^T}, \mathbf{z}_{\Lambda_2}^{(k+1)^T} \right]^T = \mathcal{K}^{(k+1)} \left(\mathbf{Y}^{(k+1)} - \hat{\mathsf{Y}}^{(k+1)} \right)$, where the observation (MR signal vector) at iteration step $k+1$ is $\mathbf{Y}^{(k+1)} = \left[Y_1^{(k+1)}, \dots, Y_N^{(k+1)} \right]$, and $Y_n^{(k+1)}$ is given by equation (5).
3. Compute the posterior estimates:
$\left(\hat{\mathbf{U}}_i^{(k+1)}, \hat{\Lambda}_i^{(k+1)} \right) = \mathrm{Exp}_{\left(\hat{\mathsf{U}}_i^{(k+1)}, \hat{\Lambda}_i^{(k+1)} \right)} \left(\mathbf{z}_{\mathbf{U}_i}^{(k+1)^T}, \mathbf{z}_{\Lambda_i}^{(k+1)^T} \right)$

of proposed technique w.r.t. the ground truth. The second experiment involves results obtained by applying our method to the fiber cup challenge phantom [7], which has been widely used by numerous research groups across the world to evaluate their tractography methods. We present our results along with quantitative comparisons to those reported in [7]. Finally, we present results obtained on a real dataset used in the MICCAI'12 tractography challenge [19].

3.1. Synthetic Data Experiments

In this experiment, we generated synthetic datasets containing 2 fiber bundles, crossing at various angles

$\{45, 60, 75, 90\}$. Then, we corrupted each data by Riccian noise at 3 different levels, i.e., $SNR \approx 7, 12, 17$. We compared proposed method with 2 existing recursive filter-based approaches (UKF & IUKF) [14, 5]. For each method, we computed the spatial distances of each fiber to the ground truth, using the error measure introduced in [7]. Fig. 2 shows the mean error of each method, for different angles and noise levels. It is evident that our method provides a more accurate estimation compared to the competing methods. We now present tractography results from
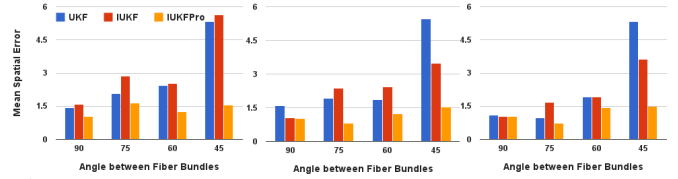

Figure 2: Comparison of accuracy of IUKFPro, IUKF & UKF. The SNRs are 17, 12 & 7 from left to right, respectively.

an application of IUKFPro to the fiber cup phantom [7], along with the quantitative comparisons to other tractography methods [20, 11, 21, 14], three of who were winners of the challenge [7]. The phantom simulates a coronal section of the human brain, including various kissing and crossing fiber bundles with different curvatures. For the acquisition parameters, we refer the reader to [7]. Fig. 3 depicts the fiber tracts obtained using our method (IUKFPro) as well as other competing algorithms. For quantitative validation, we computed the spatial, angular and curvature distances, described in [7], between the estimated fibers from each method and the ground truth.

Fig. 4 depicts the errors computed from our method compared to the first [20], second [11] and third [14] winners of fiber cup challenge, which are labeled as MoG, FOD and UKF, respectively. For the sake of completeness, we also compared our method to the algorithms in [5] and [21], denoted by IUKF and PAS, respectively. It can be seen that the IUKFPro outperforms the winners of the fiber cup challenge – in spatial distance and is competitive with respect to the angular and curvature measures. Moreover, it can be observed that IUKFPro provides reasonably small standard deviations in all error measures, compared to other competing methods. Further, IUKFPro is better than the other recursive filter based approaches in [14, 5], one of which was rated 3rd in the fiber cup challenge competition.

3.2. Real Data Experiments

We evaluated the effectiveness of our new tractography method on a patient's human brain scan acquired for the challenge at MICCAI'12, using 31 gradient directions. The acquisition parameters were, $b = 1000s/mm^2$, TR = 14000 ms, TE = 30 ms, FOV = 25.6 cm, with 1.0 mm voxel size and 2.6 mm slice thickness. See [19] for more details on
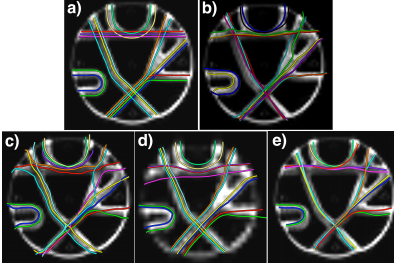
Figure 3: Tractography results obtained on the fiber cup phantom data [7]. (a) Ground-truth, (b) IUKFPro, (c) UKF [14], (d) FOD-SH [11] and (e) MoG [20].
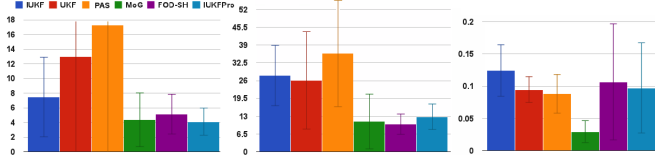

Figure 4: Quantitative comparison between IUKFPro and competing methods for the fiber cup data. Left, middle and right show the average spatial, angular and curvature distances, respectively.
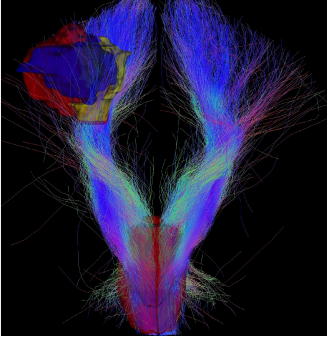

Figure 5: Tractography results using IUKFPro on the human brain dataset, depicting the corticospinal tract (CST). Brain stem is shown in red. Segmented regions at the top shown in red, blue and yellow represent the tumor, cavity and gliosis, respectively & were part of the input from [19].

the data acquisition. In this experiment, we tracked the corticospinal fibers, originating in the brain stem. Left plate in Fig. 5 depicts the estimated fibers along with the seeding region and the tumor. It can be seen from the figure that starting from the brain stem, tracts reach multiple regions of motor cortex, as expected. Further, as expected, there is a good number of tracts reaching the motor cortex on the healthy side, and a good number of tracts reconstructed on the pathological side.

4. Conclusions

In this paper, we presented novel fiber tractography algorithm by separating shape and orientation and formulating the problem of tractography on the product space of shape and orientation. By doing so, it is easier to approximately preserve clinically useful properties like anisotropy that is a key feature useful in achieving accurate tractography. We derived a novel dynamic IUKF on the product manifold of shape & orientation. Further, we presented compelling results on the fiber cup challenge phantom data [7] wherein, IUKFPro yielded smaller error than the winners of the fiber cup challenge competition. We also presented results on human brain scans that match expectations from experts.

References

[1] A. Barmpoutis et al. Regularized positive-definite fourth order tensor field estimation from DW-MRI. *NI*, 2009.

[2] P. J. Basser et al. Microstructural and physiological features of tissues elucidated by quantitative-diffusion-tensor mri. *Journal of Magnetic Resonance, Series B*, 1996.

[3] T. Behrens et al. Probabilistic diffusion tractography with multiple fibre orientations: What can we gain? *NI*, 2007.

[4] H. E. Cetingul et al. Group action induced averaging for hardi processing. In *ISBI*, 2012.

[5] G. Cheng et al. A novel intrinsic unscented kalman filter for tractography from hardi. In *ISBI*, 2012.

[6] J. Cheng et al. A riemannian framework for orientation distribution function computing. *MICCAI*, 2009.

[7] P. Fillard et al. Quantitative evaluation of 10 tractography algorithms on a realistic diffusion mr phantom. *NI*, 2011.

[8] P. Hagmann et al. Diffusion spectrum imaging tractography in complex cerebral white matter: an investigation of the centrum semiovale. In *ISMRM*, 2004.

[9] X. Hao et al. Adaptive riemannian metrics for improved geodesic tracking of white matter. In *IPMI*. Springer, 2011.

[10] S. Hauberg et al. Unscented Kalman filtering on Riemannian manifolds. *J. of Math. Img. and Vision*, 2013.

[11] B. Jeurissen et al. Fiber tracking on the fiber cup phantomusing constrained spherical deconvolution. In *MICCAI Workshop on DMFC*, 2009.

[12] S. J. Julier and J. K. Uhlmann. Unscented filtering and nonlinear estimation. *Proc. of the IEEE*, 2004.

[13] J. M. Lee. *Riemannian Manifolds: An Introduction to Curvature*. Springer, 1997.

[14] J. G. Malcolm et al. Filtered multi-tensor tractography. *IEEE TMI*, 2010.

[15] T. McGraw et al. Dt-mri denoising and neuronal fiber tracking. *MedIA*, 2004.

[16] M. Moakher. A differential geometric approach to the geometric mean of symmetric positive-definite matrices. *SIAM J. MATRIX ANAL. APPL.*, 26:735–747, 2005.

[17] S. Ncube and A. Srivastava. A novel riemannian metric for analyzing hardi data. In *SPIE Conference Series*, 2011.

[18] L. ODonnell et al. New approaches to estimation of white matter connectivity in diffusion tensor mri: Elliptic pdes and geodesics in a tensor-warped space. *MICCAI*, 2002.

[19] S. Pujol et al. Miccai dti tractography challenge - 2nd edition. In *Proc. of Int. Conf. on MICCAI*, 2012.

[20] M. Reisert et al. Tracking a physical phantom by global fibre reconstruction. *MICCAI Workshop on DMFC*, 2009.

[21] K. Sakaie. Fast persistent angular structure based streamline tractography. In *MICCAI Workshop on DMFC*, 2009.

[22] D. S. Tuch. *Diffusion MRI of complex tissue structure*. PhD thesis, Citeseer, 2002.

[23] A. Tyagi and J. W. Davis. A recursive filter for linear systems on riemannian manifolds. In *CVPR*, 2008.

[24] R. Van Der Merwe. *Sigma-point kalman filters for probabilistic inference in dynamic state-space models*. PhD thesis, University of Stellenbosch, 2004.